Contemporary Mathematics
http://ojs.wiserpub.com/index.php/CM/

Research Article

MGT Photothermal Model Incorporating a Generalized Caputo Fractional Derivative with a Tempering Parameter: Application to an Unbounded Semiconductor Medium

Ahmed E. Abouelregal[1,2], Yazeed Alhassan[1], Salman S. Alsaeed [1], Marin Marin[3,4*], Mohamed E. Elzayady[2]

[1] Department of Mathematics, College of Science, Jouf University, Sakaka, 2014, Saudi Arabia
[2] Department of Mathematics, Faculty of Science, Mansoura University, Mansoura, 35516, Egypt
[3] Department of Mathematics and Computer Science, Transilvania University of Brasov, Brasov, 500036, Romania
[4] Academy of Romanian Scientists, Ilfov Street, 3, Bucharest, 050045, Romania
E-mail: m.marin@unitbv.ro

Received: 3 September 2024; **Revised:** 21 November 2024; **Accepted:** 21 November 2024

Abstract: This work introduces a novel approach to modeling the photothermal behavior of semiconducting materials by developing a Moore-Gibson-Thompson (MGT) fractional photothermal model that incorporates a generalized Caputo fractional derivative with a tempering parameter. This advanced model is specifically designed to analyze elastic plasmonic wave systems in photothermal environments, offering deeper insights into the interactions between thermal, mechanical, and electromagnetic fields in semiconductors. By including the two-parameter tempered-Caputo fractional derivative, the model accounts for memory effects inherent in the thermal and mechanical behavior of materials exposed to high-energy processes. The model is applied to an infinite semiconducting medium with a drag-free spherical cavity subjected to a dynamically changing thermal field. This setup is highly relevant to semiconductor technology applications, where precise control over thermal and mechanical responses is crucial. The findings of this study could have significant implications for the design and analysis of semiconductor devices, particularly those operating under extreme thermal or electromagnetic conditions.

***Keywords*:** tempered-caputo, fractional derivative, photothermal analysis, semiconducting material, MGT model

MSC: 26A33, 34A08, 34K37, 35R11, 74S40

Abbreviation

The variables, parameters, and key terms involved in the governing equations used in the study of thermoelasticity, semiconductor physics, and coupled mechanical, thermal, and electronic systems can be summarized as follows:

DOI: https://doi.org/10.37256/cm.5420245963

σ_{ij}	Stress tensor components
κ	Thermal activation coupling
ρ	Material density
C_E	Specific heat
u_i	Displacement components
Q	Heat source
F_i	Body force components
G	Carrier photogeneration source
e_{ij}	Strain tensor components
D_{Eij}	Diffusion coefficients
$e_{kk} = e$	Cubical dilatation
δ_{nij}	Coupling coefficient for electronic deformation
$\theta = T - T_0$	Temperature change
N	Carier density
T_0	Reference temperature
$i,\ j,\ k$	1, 2, 3
τ	Lifetime of Photogenerated ElectronHole Pairs
K_{ij}	Thermal conductivity tensor
$\beta_{ij} = \beta_i \delta_{ij}$	Thermoelastic coupling coefficients
$\vec{q}$	Heat flux
C_{ijkl}	Elastic stiffness tensor
τ_0	Thermal relaxation
K^*_{ij}	Thermal conductivity rate
δ_{ij}	Kronecker delta
$\vec{J}$	Current density
$\vec{E}$	Induced electric field
$\vec{h}$	Induced magnetic field
$\vec{H}$	Intensity of the extemalmagnetic field
μ_0	Magnetic permeability of free space
$\lambda,\ \mu$	Lamé parameters
α_t	Thermal expansion coefficient
δ_n	Coefficient related to the carrier concentration N

1. Introduction

The photoacoustic (PA) effect, which generates acoustic waves following the absorption of light by a material, is a powerful technique that integrates optics and acoustics. It is particularly effective for examining the thermal and elastic properties of materials, making it a valuable tool in both biomedical and materials science fields [1]. In PA imaging and spectroscopy, materials absorb short laser pulses, leading to rapid thermal expansion and the creation of ultrasonic waves. These waves carry crucial information about the material's optical absorption and mechanical properties, providing insights that are often difficult to obtain through other techniques. The ability to non-invasively image and analyze tissues with high resolution and contrast makes PA methods especially useful in medical diagnostics, such as tumor detection or monitoring tissue oxygenation [2].

A thorough understanding of the physics behind thermal and elastic wave propagation in materials is essential for refining PA imaging and spectroscopy techniques. This involves studying how different materials respond to light absorption, how the generated heat affects the material's structure, and how the resulting acoustic waves propagate and are detected. By mastering these factors, researchers can fine-tune PA methods to achieve precise measurements and produce high-quality images, enhancing their utility in fields like cancer detection, tissue engineering, and the development of

advanced materials [3]. The interdisciplinary nature of PA technology also allows it to be adapted for a wide range of materials, from biological tissues to semiconductors and nanomaterials. This versatility makes it an invaluable tool for both scientific research and industrial applications, where precise measurement and control of material properties are crucial [4].

The photoacoustic (PA) effect is widely utilized in both biomedical imaging and materials science, where it serves as a powerful tool for visualization and characterization. In biomedical imaging, PA imaging is commonly used to obtain detailed images of tissue structures, blood vessels, and tumors with outstanding contrast and resolution. This technique is particularly effective for visualizing chromophores like hemoglobin and melanin, which absorb light strongly, making these components within tissues highly visible [5]. Additionally, PA imaging can provide functional data by employing different wavelengths of light to measure parameters such as blood oxygenation levels, differentiate between oxy- and deoxy-hemoglobin, and monitor metabolic activity. This makes it an indispensable tool for functional imaging in medical diagnostics [6].

In materials science, PA spectroscopy plays a crucial role in non-destructive testing, where it is used to identify defects, inhomogeneities, and stress distributions within materials. The sensitivity of PA techniques to both thermal and mechanical properties enable a comprehensive evaluation of material quality and performance. Additionally, PA methods are employed in the study of nanomaterials, such as nanoparticles and thin films, to investigate their thermal and optical properties [7]. These insights are vital for advancing applications in electronics, photonics, and energy harvesting, where accurate material characterization is essential for innovation and progress.

Thermoelasticity is fundamental in a range of fields, including geophysics, aeronautical engineering, and materials research. It offers a theoretical foundation for understanding how materials react to mechanical and thermal forces, which is vital in disciplines where temperature changes significantly influence the mechanical behavior of substances. Fields such as materials science, spacecraft design, structural engineering, and geophysical sciences depend heavily on thermoelasticity [8]. In these areas, materials are often exposed to both mechanical and thermal stresses, making a thorough understanding of thermoelastic properties crucial for designing structures and systems capable of enduring such conditions [9].

In traditional heat conduction theory, the Fourier heat equation [10] posits that heat flow is directly proportional to the temperature gradient, which implies that heat waves propagate at an infinite speed. However, this assumption is not physically accurate, as heat transmission in materials occurs at a finite speed. The notion of infinite propagation speed suggested by Fourier's law is a notable limitation, particularly in cases involving rapid thermal processes or materials with low thermal diffusivity [11].

To overcome this limitation, the hyperbolic heat transfer equation provides a more accurate model of heat conduction, especially for thermal wave phenomena in materials. Unlike Fourier's law, the hyperbolic heat transfer equation accounts for the finite speed of thermal wave propagation, offering a more realistic approach to modeling heat transfer [12, 13]. This equation is especially valuable in contexts where thermal inertia plays a significant role, such as in high-speed thermal processes or in materials with high thermal conductivity and specific heat.

Generalized thermoelasticity models expand upon traditional elasticity theory by integrating temperature effects [14–17]. These models offer a more detailed understanding of how materials respond when subjected to both mechanical stresses and temperature fluctuations. In thermoelasticity, the interaction between thermal and mechanical fields is vital, as temperature changes can generate mechanical stresses, while mechanical deformation can, in turn, influence the temperature distribution within a material. A breakthrough in thermoelasticity was achieved by Tzou [18, 19], who introduced the dual-phase lag (DPL) thermoelastic model. This innovative approach improves upon the traditional Fourier heat conduction model by incorporating two distinct time delays, or phase lags: one for the heat flux and another for the temperature gradient.

The DPL model overcomes the limitations of Fourier's law by recognizing that neither the heat flow nor the temperature gradient responds instantaneously to changes in thermal conditions. Instead, there is a time delay between the cause (such as a sudden temperature shift) and the resulting effect (such as the subsequent heat flow) [20]. By accounting for these dual-phase lags, the DPL model offers a more precise understanding of the thermal behavior of thermoelastic materials, particularly under conditions of dynamic thermal loading. The DPL model is especially valuable in situations

involving rapid thermal processes, such as laser-material interactions, high-speed machining, or pulsed thermal loading. It enables more precise predictions of temperature fields and thermal stresses, which are essential for designing materials and structures capable of enduring extreme thermal conditions [21].

Fractional models have become increasingly popular across various scientific and engineering fields due to their ability to accurately represent complex system behaviors that traditional integer-order models often cannot capture. These models are especially useful for describing phenomena that exhibit memory effects, power-law behavior, and non-local dependencies, which are common in systems with intricate dynamics. Consequently, fractional calculus and fractional differential equations have emerged as essential tools in disciplines such as mechanics, thermodynamics, electrical engineering, and control theory, among others [22, 23].

Fractional models are increasingly used to describe a variety of physical and engineering phenomena that classical approaches often fail to adequately capture. In the case of anomalous diffusion, where deviations from classical Brownian motion are observed in heterogeneous or disordered media like porous materials [24, 25] and biological tissues [26, 27], fractional diffusion equations offer a more precise description. These equations use fractional derivatives to capture processes like long-range correlations and memory effects, effectively modeling sub-diffusive and super-diffusive behaviors often seen in real-world systems [28].

In the study of viscoelasticity, where materials exhibit both elastic and viscous behavior with time-dependent strain, traditional models such as Maxwell and Kelvin-Voigt often prove insufficient. Fractional-order viscoelasticity models, which incorporate fractional derivatives, provide a more accurate representation by capturing the wide range of relaxation and creep behaviors observed in polymers and biological tissues [29]. For fractional advection-dispersion processes, which describe the transport of particles or substances in a flowing medium, traditional models typically assume Gaussian distributions and linear mechanisms. However, fractional advection-dispersion equations with space and time fractional derivatives offer a more realistic depiction of transport processes that exhibit anomalous spreading or retention, particularly in fractured rocks and complex fluids [30].

Fractional differential equations are central to the application of fractional models. These equations generalize classical differential equations by allowing the order of differentiation to be a non-integer (fractional) value. The most used fractional derivatives include the Riemann-Liouville, Caputo, and Grnwald-Letnikov derivatives, each providing different advantages depending on the specific application [31, 32]. The Riemann-Liouville derivative is often used for theoretical development in fractional calculus, as it is well-suited for problems where the initial conditions are given in terms of fractional integrals. The Caputo derivative is preferred in engineering applications because it allows the initial conditions to be specified in the same way as classical differential equations (i.e., in terms of integer-order derivatives). The Grnwald-Letnikov derivative is commonly used in numerical simulations, as it is defined through a discrete convolution sum, making it suitable for approximating solutions to fractional differential equations [33].

Recent advancements in fractional calculus, especially the development of derivatives with non-singular kernels, have broadened the analytical tools available for studying complex systems and dynamic processes. These innovations enable researchers to more accurately model and understand a variety of phenomena, providing deeper insights into the behavior of systems with non-local, memory-dependent, or dissipative properties. The Caputo-Fabrizio derivative [34, 35], which is extensively discussed in the literature, employs an exponential law kernel and offers a flexible method for modeling dissipative processes, thereby improving prediction accuracy in certain situations. Meanwhile, the Atangana-Baleanu derivative [36, 37], which uses the Mittag-Leffler (ML) kernel, is noted for its enhanced capability to capture non-local and memory effects, providing significant advantages over traditional derivatives that rely on singular kernels.

In materials science, the Caputo tempered fractional derivative has emerged as a crucial tool for modeling complex thermal dynamics and interactions that go beyond the scope of standard fractional derivatives. This derivative not only incorporates the memory effects inherently present in many materials but also allows for the modulation of these interactions over time, making it particularly effective for analyzing the behavior of advanced materials under various thermal and mechanical conditions [38, 39]. The Caputo tempered fractional derivative is a variation of the standard Caputo fractional derivative that incorporates an exponential tempering factor to modulate the memory effects typical of fractional calculus. This tempering factor adjusts the impact of past states on the current behavior of the system, allowing

for a more flexible and precise description of processes that exhibit both long-range correlations and diminishing memory effects [40, 41].

The main goal of this work is to introduce an advanced photothermal model that utilizes tempered Caputo (CT) fractional derivatives to examine the behavior of semiconductors, specifically those with spherical cavities. The CT fractional derivative is a powerful tool in materials science, offering enhanced capabilities for modeling complex thermal dynamics and interactions that surpass the limitations of standard fractional derivatives The CT fractional derivative's ability to incorporate memory effects and adjust interactions over time makes it particularly effective for analyzing advanced materials, where traditional models often fall short. This study aims to overcome the limitations of conventional photothermal models, particularly in handling non-local and memory effects that emerge under extreme thermal conditions. The research provides new insights into how fractional calculus can enhance the modeling of photothermal response and optical excitation, especially in scenarios involving non-local effects and memory-dependent behavior.

2. Mathematical formulation

In the study of thermoelasticity and electronic deformation processes, the interaction between thermal and mechanical deformations, as well as the influence of external forces, is critical. These interactions are described through the equations of motion, which capture the behavior of materials under the combined effects of mechanical loads, thermal stresses, and electronic deformations. The specific form of these equations depends on the assumptions and simplifications made during the modeling process.

The governing equations describing the behavior of thermoelastic and electronic deformation processes in a semiconductor material subjected to external forces, thermal effects and electronic interactions can be expressed as follows [42–44]:

The constitutive equation in a thermoelastic material with electronic deformation:

$$\sigma_{ij} = C_{ijkl} e_{kl} - (\beta_{ij}\theta + \delta_{nij} N). \tag{1}$$

The strain-displacement relation:

$$e_{ij} = \frac{1}{2}\left(u_{i,\,j} + u_{j,\,i}\right). \tag{2}$$

The equation of motion, including the effects of external force:

$$\sigma_{ij,\,j} + F_i = \rho \ddot{u}_i. \tag{3}$$

The increase in carrier density N due to the linked plasma-thermal-elastic wave equation:

$$\left(D_{E_{ij}} N_{,\,j}\right)_{,\,i} = \rho \frac{\partial N}{\partial t} + \frac{1}{\tau} N + \kappa\theta + G. \tag{4}$$

Energy balance equation for heat conduction:

$$\rho C_E \frac{\partial \theta}{\partial t} + T_0 \frac{\partial}{\partial t}(\beta_{ij} e_{ij}) = -\vec{\nabla} \bullet \vec{q} + Q. \tag{5}$$

Conventional Fourier's law describes heat conduction as a process where the heat flux $\vec{q}$ is proportional to the negative gradient of temperature $\vec{\nabla}\theta$, expressed as $\vec{q} = -K_{ij}\vec{\nabla}\theta$. However, a significant limitation of Fourier's law is that it predicts an infinite speed of heat propagation, which is physically unrealistic, especially in scenarios involving high-rate transient heat transfer or in materials with low thermal conductivity.

To address this issue, the Cattaneo-Vernotte (CV) modification introduces a time-relaxation term τ_0 into the heat conduction equation. This addition serves to limit the speed of heat propagation, thereby making the model more physically accurate for transient heat conduction scenarios [45]. The modified heat conduction law is given by [45]:

$$(1 + \tau_0 \frac{\partial}{\partial t})\vec{q} = -K_{ij}\vec{\nabla}\theta. \tag{6}$$

The Green and Naghdi (GN) models extend thermoelasticity theories by incorporating the concept of thermal displacement T_d, which interacts with both the mechanical displacement and temperature fields [15, 16]. In the GN-III model, an additional term $K^*_{ij}\vec{\nabla}T_d$ is introduced into the heat flux equation. This leads to the equation [15]:

$$\vec{q} = -K_{ij}\vec{\nabla}\theta - K^*_{ij}\vec{\nabla}T_d, \tag{7}$$

where the time derivative of the thermal displacement T_d equals the temperature θ.

When dealing with semiconductor materials, particularly those influenced by plasma effects, the heat conduction equation becomes more complex due to the interaction between the thermal field, electronic deformation, and plasma waves. The modified Fourier law for semiconductors under plasma influence includes a photo-excitation term [46, 47]:

$$\vec{q} = -K_{ij}\vec{\nabla}\theta - K^*_{ij}\vec{\nabla}T_d - \int \frac{E_g}{\tau} N d\vec{x}. \tag{8}$$

This equation captures the intricate interaction between thermal and electronic phenomena in semiconductors, with the final term representing the impact of photoexcitation on heat conduction. This is especially important in situations where light beams are absorbed by the semiconductor, resulting in the generation of free carriers, which in turn lead to electronic deformation and elastic vibrations [48].

Building on the Cattaneo-Vernotte framework, the improved Fourier law (8) with semiconductor effects can be expressed as [49, 50]:

$$\left(1 + \tau_0 \frac{\partial}{\partial t}\right)\vec{q} = -K_{ij}\vec{\nabla}\theta - K^*_{ij}\vec{\nabla}T_d - \int \frac{E_g}{\tau} N d\vec{x}. \tag{9}$$

Differentiating this equation with respect to spatial coordinates $\vec{x}$ yields:

$$\left(1 + \tau_0 \frac{\partial}{\partial t}\right)\left(\vec{\nabla} \bullet \vec{q}\right) = -\vec{\nabla} \bullet \left(K_{ij}\vec{\nabla}\theta\right) - \vec{\nabla} \bullet \left(K^*_{ij}\vec{\nabla}T_d\right) - \frac{E_g}{\tau} N. \tag{10}$$

Fractional derivatives offer a powerful framework for modeling systems with memory and hereditary effects, deepening our understanding of complex dynamics in fields such as heat transfer and viscoelasticity. Traditional heat conduction models, like those based on Fourier's law, often assume instantaneous heat propagation, which can be inaccurate when dealing with materials that exhibit memory effects or non-local interactions. Fractional derivatives enable the generalization of these models to incorporate such effects. In particular, the fractional derivative operator D_t^{α} with order $\alpha \in (0,1)$ is introduced to refine and enhance classical heat conduction models.

Equation (10) can be extended by incorporating the fractional derivative D_t^{α} into the heat equation, modifying the time-dependent term to account for memory effects [51, 52].

$$(1+\tau_0^{\alpha} D_t^{\alpha})\left(\overrightarrow{\nabla} \bullet \overrightarrow{q}\right) = -\overrightarrow{\nabla} \bullet \left(K_{ij} \overrightarrow{\nabla} \theta\right) - \overrightarrow{\nabla} \bullet \left(K_{ij}^{*} \overrightarrow{\nabla} T_d\right) - \frac{E_g}{\tau} N. \tag{11}$$

In this context, $D_t^{(\alpha)}$ refers to a fractional derivative operator, which can take on various forms depending on the specific formulation used. These forms may include:

- The Caputo Fractional Derivative [53]:

$$ {}_0^C D_0^{(\alpha)} Y(t) = \frac{1}{\Gamma(1-\alpha)} \int_0^t \frac{1}{(t-s)^{\alpha}} \frac{d}{ds} Y(s) ds. \tag{12}$$

- The Atangana-Baleanu Fractional Derivative [36, 37]:

$$ {}_0^{AB} D_t^{(\alpha)} Y(t) = \frac{1}{1-\alpha} \int_0^t E_{\alpha}\left(-\mu_{\alpha}(t-s)^{\alpha}\right) \frac{d}{ds} Y(s) ds, \quad \alpha \in (0,\ 1), \tag{13}$$

where $\mu_{\alpha} = \dfrac{\alpha}{1-\alpha}$ and $E_{\alpha}(z) = \sum_{n=0}^{\infty} \dfrac{z^n}{\Gamma(1+\alpha n)}$ is the generalized Mittag-Leffler function-Caputo tempered (CT) fractional derivative [39, 40]:

$$ {}_0^{CT} D_t^{\alpha,\ \chi} Y(t) = \frac{e^{-\chi t}}{\Gamma(1-\alpha)} \int_0^t \frac{d}{ds}\left(e^{\chi \xi} Y(s)\right) (t-s)^{-\alpha} d\xi, \quad \alpha \in (0,\ 1). \tag{14}$$

The CT fractional derivative introduces a modification to the traditional Caputo fractional derivative by incorporating a tempering parameter $\chi \geq 0$, which adjusts the influence of the fractional derivative over time. This modification allows the derivative to model a wider range of behaviors, particularly in systems where long-term memory effects diminish over time, a common scenario in physical and engineering applications [54]. When $\chi = 0$, the CT fractional derivative simplifies to the standard Caputo fractional derivative, demonstrating that the CT derivative is a generalization that includes the Caputo derivative as a special case.

The Caputo tempered fractional derivative is particularly useful across various fields. In modeling anomalous diffusion, it helps account for diminishing memory effects over time, which is common in physical systems. In financial models, it can be applied to scenarios where the impact of historical data gradually fades [55]. For viscoelastic materials, it captures the weakening response to stress or strain over time. In signal processing, it is valuable for filtering operations where the influence of past signals decreases as they age.

Substituting the fractional derivative-based equation (11) into equation (5) results in a modified fractional heat conduction equation. This equation can be expressed as:

$$(1+\tau_0^{\alpha}D_t^{\alpha})\left[\rho C_E\frac{\partial^2\theta}{\partial t^2}+T_0\frac{\partial^2}{\partial t^2}\left(\beta_{ij}u_{i,\,j}\right)-\rho\frac{\partial Q}{\partial t}\right]=\left(K_{ij}\dot{\theta}_{,\,j}\right)_{,\,i}+\left(K_{ij}^{*}\theta_{,\,j}\right)_{,\,i}+\frac{E_g}{\tau}\frac{\partial N}{\partial t}. \tag{15}$$

This equation serves as an advanced model for heat conduction in materials where thermal, elastic, and plasma waves interact. By incorporating fractional derivatives, the model effectively captures memory effects, enhancing its accuracy in describing materials with complex thermal behavior. This equation is especially relevant in areas such as semiconductor physics, where the interplay between thermal and electronic phenomena critically influences the material's properties.

When a magnetic field is applied to semiconductor materials, it can generate both induced electric and magnetic fields, which subsequently affect the material's electrical deformation and elastic vibrations. These interactions alter the material's thermal properties, necessitating the use of Maxwell's equations to understand this complex behavior [56]. Maxwell's equations govern the interaction and evolution of electric and magnetic fields over time. When integrated with the material's mechanical and thermal properties, these equations offer a thorough framework for analyzing the impact of electromagnetic fields on semiconductors.

Maxwell's equations, in their most general form, describe the behavior of electric and magnetic fields in any medium. When applied to a semiconductor material subjected to an external magnetic field, these equations can be written as [57, 58]:

$$\overrightarrow{J}=\nabla\times\overrightarrow{h},\quad \nabla\times\overrightarrow{E}=-\mu_0\frac{\partial\overrightarrow{h}}{\partial t},\quad \overrightarrow{E}=-\mu_0\left(\frac{\partial\overrightarrow{u}}{\partial t}\times\overrightarrow{H}\right),\quad \nabla\cdot\overrightarrow{h}=0. \tag{16}$$

The Maxwell stress tensor M_{ij} quantifies the force per unit area that an electromagnetic field exerts on a material. This tensor plays a key role in analyzing how electromagnetic fields influence the mechanical properties of a material, including stress and deformation. The expression for the Maxwell stress tensor is given by [59]:

$$M_{ij}=\mu_0\left[H_ih_j+H_jh_i-H_kh_k\delta_{ij}\right]. \tag{17}$$

3. Formulation of the problem

In this scenario, we examine a flexible semiconductor medium that is infinite, isotropic, homogeneous, and fully electrically conductive. The medium features a spherical cavity with a radius R, and it is placed in a constant magnetic field (see Figure 1). The analysis is conducted using spherical coordinates $(r,\ \psi,\ \phi)$, where r indicates the radial distance from the center of the cavity, ψ is the azimuthal angle, and ϕ represents the polar angle. The inner surface of the cavity experiences time-dependent temperature fluctuations $f(t)$. Moreover, the cavity's surface is free of traction, meaning that the stress components on the surface are zero. A constant magnetic field, $\overrightarrow{H_0}=(0,\ 0,\ H_0)$, is applied along the ϕ-axis, which corresponds to the polar axis in the spherical coordinate system. There are no internal heat sources within the medium, so $Q=0$. Also, the medium is initially undisturbed, with no prior thermal or mechanical activity. The only body forces present in the medium are Lorentz forces, which arise from the interaction between the induced current in the semiconductor and the applied magnetic field.

Spherical symmetry will be considered, meaning the displacement vector depends solely on the radial distance r and time t, but not on the angular coordinates ψ or ϕ. Therefore, in a spherically symmetric problem, the displacement vector $\overrightarrow{u}$ in spherical coordinates simplifies to the following form:

$$\vec{u} = \begin{pmatrix} u_r \\ u_\psi \\ u_\phi \end{pmatrix} = \begin{pmatrix} u(r,\, t) \\ 0 \\ 0 \end{pmatrix}. \tag{18}$$

The non-zero strain components are derived using the strain-displacement relations from equation (2) as follows:

$$\begin{pmatrix} e_{rr} & e_{\psi\psi} & e_{\phi\phi} \end{pmatrix} = \begin{pmatrix} \dfrac{\partial u}{\partial r} & \dfrac{u}{r} & \dfrac{u}{r} \end{pmatrix}. \tag{19}$$

Consequently, the volumetric strain e is expressed as:

$$e = e_{rr} + e_{\psi\psi} + e_{\phi\phi} = \frac{\partial u}{\partial r} + 2\frac{u}{r} = \frac{1}{r^2}\frac{\partial \left(r^2 u\right)}{\partial r}. \tag{20}$$

Considering the symmetry and the interdependencies among stress, strain, temperature, and carrier concentration (1), the thermal stress components are expressed as follows:

$$\sigma_{rr} = (\lambda + 2\mu)\frac{\partial u}{\partial r} + 2\lambda\frac{u}{r} - (3\lambda + 2\mu)\left(\alpha_t \theta + \delta_n N\right), \tag{21}$$

$$\sigma_{\psi\psi} = \sigma_{\phi\phi} = \lambda\frac{\partial u}{\partial r} + 2(\mu + \lambda)\frac{u}{r} - (3\lambda + 2\mu)\left(\alpha_t \theta + \delta_n N\right), \tag{22}$$

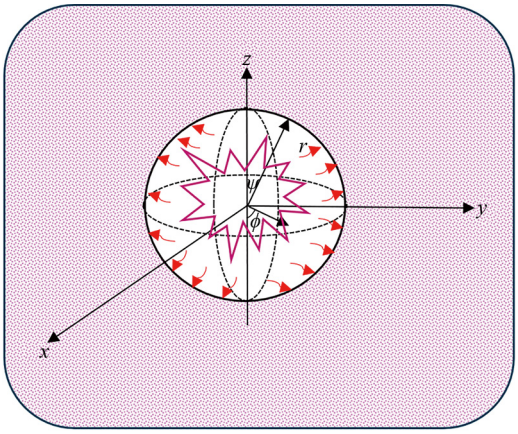

Figure 1. Schematic illustration of unbounded semiconductor with a spherical cavity

Using the relationships in equation (16), we can derive the following expressions:

$$\vec{E} = \left(0,\, \mu_0 H_0 \frac{\partial u}{\partial t},\, 0\right),\ \vec{J} = \left(0,\, \frac{\partial}{\partial r}\left(\frac{1}{r^2}\frac{\partial \left(r^2 u\right)}{\partial r}\right),\, 0\right),\ \vec{h} = \left(0,\, 0,\, \frac{1}{r^2}\frac{\partial \left(r^2 u\right)}{\partial r}\right). \tag{23}$$

The extemal magnetic field $\vec{H}_0$ induces a radial component of the Lorentz force F_r, expressed as:

$$F_r = \mu_0 \left(\vec{J} \times \vec{H}_0 \right)_r. \tag{24}$$

Using the expressions for $\vec{J}$ and $\vec{H}_0$, the radial component of the Lorentz force F_r and the Maxwell pressure M_{rr} can be calculated as follows:

$$F_r = \mu_0 H_0^2 \frac{\partial}{\partial r} \left(\frac{1}{r^2} \frac{\partial \left(r^2 u \right)}{\partial r} \right), \quad M_{rr} = \frac{\mu_0 H_0^2}{r^2} \frac{\partial \left(r^2 u \right)}{\partial r}. \tag{25}$$

Considering the radial component of Lorentz force F_r, the equation motion is given by:

$$\frac{\partial}{\partial r} \left(\sigma_{rr} \right) + \frac{2 \left(\sigma_{rr} - \sigma_{\psi\psi} \right)}{r} + \mu_0 H_0^2 \frac{\partial}{\partial r} \left(\frac{1}{r^2} \frac{\partial \left(r^2 u \right)}{\partial r} \right) = \rho \frac{\partial^2 u}{\partial t^2}. \tag{26}$$

By substituting equations (21) and (22) into equation (26), we obtain the modified equation:

$$\left(\lambda + 2\mu + \mu_0 H_0^2 \right) \frac{\partial}{\partial r} \left(\frac{1}{r^2} \frac{\partial \left(r^2 u \right)}{\partial r} \right) - \gamma \frac{\partial \theta}{\partial r} - d_n \frac{\partial N}{\partial r} = \rho \frac{\partial^2 u}{\partial t^2}. \tag{27}$$

Here, γ and d_n are defined as $(3\lambda + 2\mu)\alpha_t$ and $(3\lambda + 2\mu)\delta_n$, respectively. Equation (27) can be reformulated in terms of volumetric strain e as:

$$\left[\left(\lambda + 2\mu + \mu_0 H_0^2 \right) \nabla^2 - \rho \frac{\partial^2}{\partial t^2} \right] e = \nabla^2 \left[\gamma \theta + d_n N \right]. \tag{28}$$

where $\nabla^2 = \frac{1}{r^2} \frac{\partial}{\partial r} \left(r^2 \frac{\partial}{\partial r} \right)$.

The modified fractional (MGT) heat transfer equation, incorporating different fractional operators (C, AB, or CT) to include non-local and memory effects, can be expressed as:

$$\left(1 + \tau_0^{\alpha} D_t^{\alpha} \right) \frac{\partial^2}{\partial t^2} \left[\rho C_E \theta + \gamma T_0 e \right] - \frac{1}{\tau} E_g \frac{\partial N}{\partial t} = \left[K^* + K \frac{\partial}{\partial t} \right] \left[\frac{1}{r^2} \frac{\partial}{\partial r} \left(r^2 \frac{\partial \theta}{\partial r} \right) \right]. \tag{29}$$

The plasma-thermal-elastic wave equation (4), which describes the interaction among carrier density N, temperature θ, and mechanical deformations within a material without external carrier generation ($G = 0$), can be expressed as:

$$\left[D_E \nabla^2 - \rho \frac{\partial}{\partial t} - \frac{1}{\tau} \right] N = \kappa \theta. \tag{30}$$

Using dimensionless variables streamlines and broadens the goveming equations, facilitating the analysis and comparison of different solutions while highlighting the key factors that influence system behavior. The dimensionless variables employed in this analysis are defined as follows:

$$\{r',\, u'\} = \mathrm{v}_0\eta\{r,\, u\},\ \ \{t',\, \tau',\, \tau_0'\} = \mathrm{v}_0^2\eta\,\{t,\, \tau,\, \tau_0\},\ \ \{\theta',\, N'\} = \frac{1}{\rho\mathrm{v}_0^2}\{\gamma\theta,\, d_{\mathrm{n}}N\},$$
$$\{\sigma_{ij}',\, M_{rr}'\} = \frac{1}{\rho\mathrm{v}_0^2}\{\sigma_{ij},\, M_{rr}\},\ \ \mathrm{v}_0^2 = \mathrm{v}_{\mathrm{e}}^2 + \mathrm{v}_a^2,\ \ \eta = \frac{\rho C_E}{K}, \tag{31}$$

in which $\mathrm{v}_{\mathrm{e}} = \sqrt{\dfrac{\lambda+2\mu}{\rho}}$ denotes the speed of longitudinal elastic waves and $\mathrm{v}_a = \sqrt{\dfrac{\mu_0 H_0^2}{\rho}}$ is the Alfvn wave speed.

After applying the necessary transformations and substituting the dimensionless variables into the goveming equations, the following dimensionless forms of the equations are derived (with primes omitted):

$$(1+\tau_0^{\alpha}D_t^{\alpha})\,\frac{\partial^2}{\partial t^2}\left[\theta+\varepsilon_1 e\right] - \varepsilon_2\frac{\partial N}{\partial t} = \left[\frac{\partial}{\partial t} + g_0\right]\nabla^2\theta, \tag{32}$$

$$\left[\nabla^2 - \frac{\partial^2}{\partial t^2}\right] e = \nabla^2\Theta, \tag{33}$$

$$\left[\nabla^2 - b_1 - b_2\frac{\partial}{\partial t}\right] N = b_3\theta, \tag{34}$$

$$\sigma_{rr} = g_1\frac{1}{r^2}\frac{\partial\left(r^2u\right)}{\partial r} + g_2\frac{\partial u}{\partial r} - \Theta, \tag{35}$$

$$\sigma_{\psi\psi} = g_1\frac{1}{r^2}\frac{\partial\left(r^2u\right)}{\partial r} + g_2\frac{u}{r} - \Theta. \tag{36}$$

in which $\Theta = \theta + N$ and the following dimensionless parameters are defined:

$$g_1 = \frac{\mathrm{v}_1^2}{\mathrm{v}_0^2},\ \ g_2 = 2\frac{\mathrm{v}_2^2}{\mathrm{v}_0^2},\ \ \varepsilon_1 = \frac{\gamma^2 T_0}{C_E\rho^2\mathrm{v}_0^2},\ \ \varepsilon_2 = \frac{E_g\gamma}{\rho C_E\tau d_{\mathrm{n}}},\ \ g_0 = \frac{K^*}{\eta K\mathrm{v}_0^2},$$
$$\mathrm{v}_1 = \sqrt{\frac{\lambda}{\rho}},\ \ \mathrm{v}_2 = \sqrt{\frac{\mu}{\rho}},\ \ b_1 = \frac{1}{\eta D_E\tau},\ \ b_2 = \frac{\rho}{\eta D_E},\ \ b_3 = \frac{d_n\kappa}{\gamma\eta^2 D_E\mathrm{v}_0^2}. \tag{37}$$

4. Initial and boundary conditions

In the context of the problem under discussion, initial conditions are used to define the state of the system at the initial time $t = 0$. These conditions are crucial because they set the starting point for the analysis and influence the subsequent evolution of the system. The initial conditions for the problem, as stated, are:

$$u(r,\,0)=0,\;\;\frac{\partial u(r,\,0)}{\partial r}=0,\quad N(r,\,0)=0,\;\;\frac{\partial N(r,\,0)}{\partial r}=0,$$
$$\sigma_{\psi\psi}(r,\,0)=0,\quad \theta(r,\,0)=0=\frac{\partial\theta(r,\,0)}{\partial r},\;\;\sigma_{rr}(r,\,0)=0. \tag{38}$$

The rectified sinusoidal function ensures that the temperature always remains positive. In the context of heat transfer, this type of temperature variation could represent a scenario where the heat source fluctuates cyclically but prevents the temperature from falling below a certain baseline. It will be considered that the temperature at the surface of the gap varies according to a rectified sine function with a period of $(\frac{2\pi}{\omega})$, as described by the following relation [60–62]:

$$\theta(r,\,t)=f(t)=\theta_0\,|\sin(\omega t)\,|,\;\text{at}\;r=R, \tag{39}$$

where θ_0 is the amplitude of the temperature fluctuation and ω is the angular frequency.

Rectified sinusoidal heat variation is a flexible tool in engineering, employed in processes requiring controlled, cyclic heating while preventing the temperature from dropping below a critical threshold. This approach is widely used across industries such as metal processing, electronics, material science, and thermal management, where accurate temperature control is essential to maintain the quality, reliability, and performance of components and systems.

Traction forces, in the field of mechanics, refer to the forces exerted on a surface per unit area. When a body is devoid of traction forces, it means that there are no external pressures or stresses acting on its surface, implying that the surface is free from any external force or mechanical load. When a body is described as free of traction forces, the mechanical boundary condition in this case can be expressed as:

$$\sigma_{rr}(r,\,t)=0,\;\text{at}\;r=R. \tag{40}$$

In semiconductor devices, it is essential to understand carrier diffusion, the movement of charge carriers such as electrons and holes driven by concentration gradients, and recombination, where electrons and holes neutralize each other. These processes play a critical role in designing and optimizing components like diodes, transistors, and solar cells, as they greatly affect the distribution of charge carriers within the device, influencing its response to external inputs and overall efficiency.

A commonly used boundary condition for carrier density at a surface, particularly in the context of recombination, is expressed as [62]:

$$D_E\frac{\partial N}{\partial r}=V_{sr}N\;\text{at}\;r=R, \tag{41}$$

where V_{sr} is a parameter known as the surface recombination velocity, which quantifies the rate at which carriers recombine at the surface of the semiconductor. This parameter is essential in determining the efficiency of semiconductor devices.

5. Solution using the Laplace transform technique

Applying the Laplace transform to the governing equations simplifies solving the differential equations by converting them into algebraic equations in the Laplace domain. Once these equations are solved, the inverse Laplace transform can be used to bring the solutions back into the time domain. The Laplace transform of a function is defined as:

$$\Im\left[g(r,\,t)\,\right]=\overline{g}\,(r,\,s)=\int_0^{\infty}e^{-st}g\,(r,\,t)\,dt,\quad s>0. \tag{42}$$

Applying the Laplace transform to equations (32) to (36), we obtain the following equations in the Laplace domain:

$$\varpi\varepsilon_1\overline{e}=\left(\nabla^2-\varpi\right)\overline{\theta}+\varepsilon_3\overline{N}, \tag{43}$$

$$\left(\nabla^2-s^2\right)\overline{e}=\nabla^2\overline{\Theta}, \tag{44}$$

$$\left(\nabla^2-b_4\right)\overline{N}=b_3\overline{\theta}, \tag{45}$$

$$\overline{\sigma}_{rr}=g_2\frac{d\overline{u}}{dr}+\frac{g_1}{r^2}\frac{d(r^2\overline{u})}{dr}-\overline{\Theta}, \tag{46}$$

$$\overline{\sigma}_{\psi\psi}=g_2\frac{\overline{u}}{r}+\frac{g_1}{r^2}\frac{d\left(r^2\overline{u}\right)}{dr}-\overline{\Theta}, \tag{47}$$

where $\varpi=\dfrac{s^2\left(1+\tau_0^{\alpha}\Lambda\right)}{(\mathrm{s}+g_0)}$, $\varepsilon_3=\dfrac{\varepsilon_2\mathrm{s}}{(\mathrm{s}+g_0)}$, $b_4=b_1+sb_2$, and

$$\Lambda=\begin{cases}\mathrm{s}^{\alpha} & \text{for C fractional operotor,}\\ \dfrac{s^{\alpha}}{(1-\alpha)\,s^{\alpha}+\alpha} & \text{for (AB) fractional operator,}\\ (\mathrm{s}+\chi)^{\alpha} & \text{for CT fractional operotor.}\end{cases} \tag{48}$$

Decoupling the system of equations (43)-(45) results in a higher-order differential equation that can be generalized to describe the behavior of the system in terms of key variables such as $\overline{\theta}$, $\overline{N}$, and $\overline{e}$. The resulting differential equation takes the form:

$$\left(\nabla^6-q_2\nabla^4+q_1\nabla^2-q_0\right)\left\{\overline{\theta},\,\overline{N},\,\overline{e}\right\}=0, \tag{49}$$

where the parameters q_2, q_1, and q_0 are defined by the following expressions:

$$q_2=s^2+b_7+\frac{b_6}{b_3},\ q_1=s^2b_7+b_8+\frac{b_6b_5}{b_3},\ q_0=s^2b_8, \tag{50}$$

and the intermediate parameters b_5, b_6, b_7, and b_8 are given by:

$$\begin{aligned} &b_5=b_4-b_3,\ b_6=b_3\varpi\varepsilon_1,\\ &b_7=b_4+\varpi,\ \ b_8=b_4\varpi+b_3\varepsilon_3. \end{aligned} \tag{51}$$

To solve equation (49), we introduce the roots λ_i (where $i = 1, 2, 3$), leading to a factorization of the original sixth-order differential equation:

$$\left(\nabla^2-\lambda_1^2\right)\left(\nabla^2-\lambda_2^2\right)\left(\nabla^2-\lambda_3^2\right)\left\{\overline{e},\ \overline{\theta},\ \overline{N}\right\}=0. \tag{52}$$

Here, λ_1^2, λ_2^2 and λ_3^2 are the roots of the equation:

$$\lambda^6-q_2\lambda^3+q_1\lambda^2-q_0=0. \tag{53}$$

The general solution to differential equation (49), considering the regularity constraint, can be expressed as:

$$\left\{\overline{e},\ \overline{\theta},\ \overline{N}\right\}(r,\ s)=\frac{1}{\sqrt{r}}\sum_{i=1}^{3}\left\{1,\ L_i,\ H_i\right\}A_iK_{1/2}\left(\lambda_ir\right). \tag{54}$$

Where $K_{1/2}\left(\lambda_ir\right)$ is the hyperbolic Bessel function of the second kind of order $\frac{1}{2}$.

The parameters A_i (for $i=1, 2, 3$) are functions of the Laplace variable s, and the coefficients L_i and H_i (for $i=1, 2, 3$) are determined by:

$$H_i=\frac{b_3\lambda_i^2-s^2b_3}{\lambda_i^4-b_5\lambda_i^2},\quad L_i=\frac{H_i\lambda_i^2-b_4H_i}{b_3}. \tag{55}$$

In the Laplace domain, the relationship between $\overline{e}$ and $\overline{u}$ is given by

$$\frac{d\overline{u}}{dr}+2\frac{\overline{u}}{r}=\overline{e}. \tag{56}$$

By substituting $\overline{e}$ into equation (56) and multiplying by r^2 to simplify:

$$\frac{d}{dr}\left(r^2\overline{u}\right) = r^{3/2}\sum_{i=1}^{3} A_i K_{1/2}\left(\lambda_i r\right). \tag{57}$$

Integrate the equation (57) with respect to r, we get:

$$r^2\overline{u} = \sum_{i=1}^{3} A_i \int r^{3/2} K_{1/2}\left(\lambda_i r\right) dr = -r^{3/2}\sum_{i=1}^{3} A_i K_{3/2}\left(\lambda_i r\right)/\lambda_i. \tag{58}$$

Then final expression for the displacement $\overline{u}$ is given by

$$\overline{u} = -\frac{1}{\sqrt{r}}\sum_{i=1}^{3}\frac{1}{\lambda_i} K_{3/2}\left(\lambda_i r\right) A_i. \tag{59}$$

In the derived equation (59), the following Bessel relation is utilized:

$$\int K_{1/2}\left(\lambda_i r\right) = -\frac{1}{\lambda_i} K_{3/2}\left(\lambda_i r\right). \tag{60}$$

The modified Bessel functions of the second kind, $K_n(z)$, have specific asymptotic expressions that make them easier to evaluate for certain orders, especially for half-integer orders. For the particular cases of $K_{1/2}(z)$ and $K_{3/2}(z)$, the relations are as follows:

$$K_{\frac{1}{2}}(z) = \sqrt{\frac{\pi}{2z}}\exp(-z), \quad K_{\frac{3}{2}}(z) = \sqrt{\frac{\pi}{2z}}\exp(-z)\left(1+\frac{1}{2z}\right). \tag{61}$$

By incorporating the relations (61) into equations (54) and (59), we obtain the following:

$$\left\{\overline{e},\ \overline{\theta},\ \overline{N}\right\} = \frac{1}{r}\sum_{i=1}^{3}\left\{1,\ L_i,\ H_i\right\} A_i\sqrt{\frac{\pi}{2\lambda_i}}\exp\left(-\lambda_i r\right), \tag{62}$$

$$\overline{u} = -\sum_{i=1}^{2}\frac{1}{\lambda_i\sqrt{r}} A_i\sqrt{\frac{\pi}{2\lambda_i r}}\left(1+\frac{1}{2\lambda_i r}\right)\exp\left(-\lambda_i r\right). \tag{63}$$

Utilizing equations (46), (47), (62) and (63), the closed-form solutions for the thermal stresses $\overline{\sigma}_{rr}$ and $\overline{\sigma}_{\psi\psi}$ can be expressed as follows:

$$\overline{\sigma}_{rr}=\sqrt{\frac{\pi}{2r}}\sum_{i=1}^{3}\frac{1}{(\lambda_i r)^{5/2}}A_i\exp\left(-\lambda_i r\right)\left(2g_2+2rg_2\lambda_i+r^2(g_1+g_2-H_i-L_i)\lambda_i^2\right), \tag{64}$$

$$\overline{\sigma}_{\psi\psi}=-\sqrt{\frac{\pi}{2r}}\sum_{i=1}^{3}\frac{1}{(\lambda_i r)^{5/2}}A_i\exp\left(-\lambda_i r\right)\left(r^2(-g_1+H_i+L_i)\lambda_i^2+g_2(1+r\lambda_i)\right). \tag{65}$$

The non-dimensional transformed solution for Maxwell's stress $\overline{M}_{rr}$ can be expressed as:

$$\overline{M}_{rr}=\frac{\mathrm{v}_a^2}{\mathrm{v}_0^2}\frac{1}{\sqrt{r}}\sum_{i=1}^{3}A_i\exp\left(-\lambda_i r\right)\sqrt{\frac{\pi}{2\lambda_i r}}. \tag{66}$$

After applying the Laplace transform, the boundary conditions (39)-(41) are transformed into the following forms:

$$\overline{\theta}\left(R,\ \mathrm{s}\right)=\frac{\theta_0\omega}{\omega^2+s^2}\coth\left(\frac{\pi s}{2\omega}\right),$$

$$\overline{\sigma}_{rr}\left(R,\ \mathrm{s}\right)=0, \tag{67}$$

$$D_E\frac{\partial\overline{N}\left(R,\ s\right)}{\partial r}=V_{sr}\overline{N}\left(R,\ s\right).$$

Substituting equations (62) and (64) into equation (67) yields:

$$\sum_{i=1}^{3}L_iA_i\exp\left(-\lambda_i R\right)\sqrt{\frac{\pi}{2\lambda_i R}}=\frac{\theta_0\omega\sqrt{R}}{\omega^2+s^2}\coth\left(\frac{\pi s}{2\omega}\right), \tag{68}$$

$$\sum_{i=1}^{3}\frac{A_i}{\sqrt{R}(\lambda_i R)^{5/2}}\exp\left(-\lambda_i R\right)\left(2g_2+2Rg_2\lambda_i+R^2(g_1+g_2-H_i-L_i)\lambda_i^2\right)=0, \tag{69}$$

$$-D_E\sqrt{\frac{\pi}{2}}\sum_{i=1}^{3}\frac{H_i}{R^{3/2}\sqrt{\lambda_i R}}\exp\left(-\lambda_i R\right)\left(1+\lambda_i R\right)=\frac{V_{sr}}{\sqrt{R}}\sum_{i=1}^{3}e^{-\lambda_i R}\sqrt{\frac{\pi}{2\lambda_i R}}. \tag{70}$$

The coefficients A_i (where i= 1, 2, 3) are determined by solving the system of equations (68)-(70).

6. Inversion of Laplace transforms

Inverting Laplace transforms is essential for converting results from the frequency domain back to the time domain, enabling us to analyze the time-dependent behavior of systems. This process can be challenging, particularly when dealing with functions that have complex mathematical expressions [63, 64]. See also [65–68]. Traditional methods, such as partial fraction decomposition, the convolution theorem, or residue calculus, often demand considerable mathematical

effort and may not always be simple to apply. A more efficient way to approximate inverse Laplace transforms is by using the Fourier series expansion approach. This technique is grounded in the basic idea that any periodic function can be represented as a sum of sine and cosine functions, which form its Fourier series. By applying this concept, the inverse Laplace transform can be approximated by expressing it as a combination of these trigonometric functions. The inversion of a function $\overline{\mathscr{G}}(r,\, s)$ in the Laplace domain can be numerically achieved using the following formula [69]:

$$\mathscr{G}(r,\, t)=\frac{1}{2t}\overline{\mathscr{G}}(r,\, \mathscr{S})\, e^{\mathscr{S}t}+2\left\{\mathrm{Re}\sum_{=1}^{m}(-1)\overline{\mathscr{G}}\left(r,\, \mathscr{S}+\frac{\iota\pi}{t}\right)\frac{1}{2t}e^{\mathscr{S}t}\right\}. \tag{71}$$

The parameter $\mathscr{S}$ affects the speed at which the series converges. The variable m denotes the number of terms included in the Fourier series expansion. The notation Re refers to the real part of a complex number. The selection of $\mathscr{S}$ is crucial for the convergence of the series. Numerical experiments have shown that choosing $\mathscr{S}$ approximately as $\mathscr{S}\approx 4.7/t$ ensures rapid convergence for a wide variety of functions.

7. Special cases

The MGT fractional photothermal model, presented in this work, offers a robust framework aimed at overcoming the limitations and physical inconsistencies present in earlier photothermal elasticity models. This model integrates fractional derivatives and extends various classical and modern theories in photothermal elasticity. In this section, we examine how specific cases of this model relate to previous models by adjusting key parameters, such as τ_0, K^*, and the order of the fractional derivatives α.

7.1 *Photo-thermoelastic models with non-fractional derivatives* $(\alpha = 1)$

In the absence of fractional derivatives (when $\alpha= 1$), the MGT model simplifies to various classical photothermal elasticity models depending only on the values of τ_0 and K^*.

- Classical photothermal elasticity (PTCTE) Model ($\tau_0 = 0$ and $K^* = 0$).
- LS photothermal (PTLS) Model ($\tau_0 > 0$ and $K^* = 0$).
- GN photothermal models (PTGN-II and PTGN-III) ($\tau_0 = 0$).
- MGT photothermal Model (PTMGT) ($\tau_0 = 0$ and $K^* = 0$).

7.2 *Fractional thermoelastic models* $(0 < \alpha < 1)$

When the order of the fractional derivatives α is within the range $0 < \alpha < 1$, the MGT model generalizes to fractional photothermal models. These models introduce memory effects and non-local behavior, making them more suitable for describing complex materials and processes where classical models fall short.

- Fractional LS photothermal (PTLS) Model ($\tau_0> 0$ and $K^*= 0$).
- Fractional GN photothermal models (PTGN-II and PTGN-III) ($\tau_0= 0$).
- Fractional MGT photothermal Model (PTMGT) ($\tau_0= 0$ and $K^*= 0$).

8. Numerical results

The numerical results derived from the modified Moore-Gibson-Thompson (MGT) fractional photothermal model are displayed in both graphical and tabular formats to enable thorough analysis and interpretation. These results were generated using Mathematica, a robust tool for numerical computation and visualization. The graphs and tables not only showcase the theoretical predictions but also offer insight into the behavior of various physical fields under different

conditions. Comparing these numerical results with experimental data allows for further evaluation of the validity and accuracy of the modified MGT model.

Silicon (Si) is an ideal material for numerical analysis in semiconductor studies because of its distinctive combination of physical, electrical, and mechanical properties. Additionally, its intrinsic electrical conductivity can be precisely adjusted through doping with other elements, enabling fine control over its conductive characteristics. This adaptability makes silicon perfect for applications in transistors, diodes, and integrated circuits. Furthermore, its optical properties make it well-suited for photonic applications, such as waveguides, modulators, and sensors. The initial temperature for the analysis is established at $T_0 = 300$ K. The key physical parameters of silicon, essential for the numerical computations, are as follows:

• Mechanical Properties:

$$\lambda = \left(3.64\times10^{10}\right) \text{kg m}^{-1}\text{s}^{-2}, \quad \mu = \left(5.46\times10^{10}\right) \text{kg m}^{-1}\text{s}^{-2},$$

$$\rho = 2329 \text{ kg m}^{-3}, \quad \alpha_t = (3\times10^{-6})\text{K}^{-1}.$$

• Thermal Properties:

$$K = 148 \text{ W m}^{-1}\text{K}^{-1}, \quad C_E = \left(7.03\times10^{2}\right) \text{ J kg K}^{-1}.$$

• Electrical Properties:

$$E_g = 1.12 \text{ eV}, \quad D_E = \left(2.5\times10^{-3}\right) \text{ m}^2 \text{ s}^{-1}, \quad V_{sr} = 2 \text{ m s}^{-1},$$

$$\tau = \left(5\times10^{-5}\right) \text{ s}, \quad \delta_n = -\left(9\times10^{-31}\right) \text{ m}^3.$$

• Magnetic and Dielectric Properties:

$$H_0 = \left(10^7/4\pi\right) \text{Am}^{-1}, \ \mu_0 = \left(4\pi\times10^{-7}\right) \text{Hm}^{-1}, \ \varepsilon_0 = \left(10^{-9}/36\pi\right) \text{Fm}^{-1}.$$

The numerical method described in equation (71) was utilized to obtain the numerical results and examine the intricate interactions among thermal, plasma, and elastic waves within the framework of the fractional MGT photothermal model. This advanced analysis provides a comprehensive understanding of how different physical fields interact within the material, particularly considering the influence of fractional derivatives, which introduce memory effects and non-local behavior.

Figures 2-6 collectively illustrate the complex interactions between thermal, plasma, and elastic waves, as well as their influence on the material's mechanical and thermal response. The visual representation enhances the understanding of how coupled fields (θ, u, N, σ_{rr}, and $\sigma_{\psi\psi}$) evolve over time and space, providing a clearer picture of the underlying physical phenomena governed by the fractional MGTE photothermal model.

In advanced heat conduction models, the inclusion of fractional derivatives is crucial for capturing memory effects, which are vital for accurately representing materials with complex thermal behaviors. These fractional derivatives alter the time-dependent terms in the heat equation, offering a more detailed and accurate description of thermal processes over time. Utilizing different types of fractional derivatives, like Caputo (C), Atangana-Baleanu (AB), or Caputo tempered

(CT), allows for the modeling of a wide range of memory effects, from simple power-law decays to more intricate non-local behaviors. These advancements are vital for deepening the understanding and simulation of thermal processes in materials that display anomalous diffusion and other non-classical characteristics. In this section of the study, we will conduct a comparative analysis of the behavior of the physical fields under the influence of different fractional derivative operators: C, AB, and CT. These fractional derivatives introduce memory effects and non-local behavior into the system, which significantly impacts how physical fields such as temperature, displacement, stress, and carrier density evolve over time and space.

The goal of this comparison is to gain a deeper understanding of how each fractional operator influences the system's dynamics. Specifically, the comparison aims to explore the impact of memory effects, examining how the system's past states continue to affect its current behavior. Additionally, the analysis seeks to identify differences in the spatial and temporal response, highlighting how physical fields propagate and interact over time and across spatial domains. Finally, the comparison focuses on damping and decay, investigating how the incorporation of different fractional derivatives modifies the rate of decay and the stability of the physical fields.

The fractional PTMGT photothermal model, utilized in this comparison, stands as the most advanced, integrating relaxation time and fractional derivatives to capture a broad spectrum of thermal, mechanical, and electromagnetic interactions. This model is specifically designed to overcome the limitations of earlier models, providing a comprehensive framework that includes memory effects and non-local behavior. From Figures (2-6), the influence of fractional derivatives on the behavior of physical fields can be examined by comparing three specific models: Caputo, Atangana-Baleanu (AB), and Caputo Tempered (CT). Each of these derivatives introduces distinct memory effects and uniquely affects the evolution of temperature, displacement, stress, and carrier density fields.

Figure 2 effectively illustrates the distinct behaviors of the temperature field (θ) under different fractional derivatives. The Caputo derivative leads to smooth, prolonged temperature distributions, while the AB derivative extends this effect further, creating an even slower and broader thermal response. In contrast, the CT derivative, results in a faster temperature decline and quicker stabilization by reducing the long-term memory effect, making it ideal for systems requiring rapid thermal stabilization response. This comparative analysis highlights the importance of selecting the appropriate fractional derivative based on the specific thermal dynamics of the system being modeled.

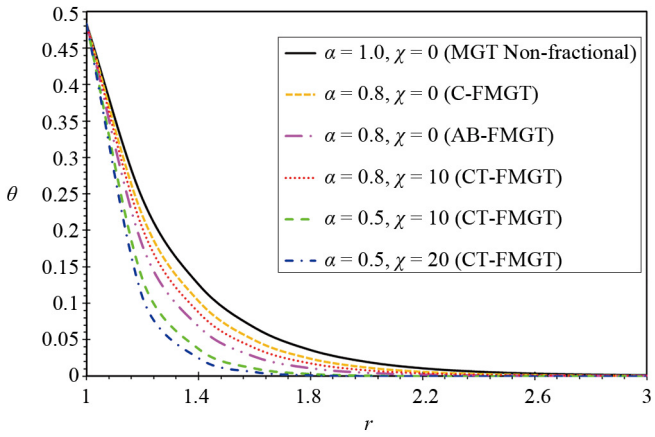

Figure 2. Temperature variation (θ) under various fractional derivative operators

The Caputo derivative introduces a power-law memory effect, where the current radial displacement u is influenced by the entire history of past deformations. This accumulated memory causes the displacement field to evolve more slowly, leading to a delayed response when forces are applied, as shown in Figure 3. This behavior is particularly relevant in materials designed to absorb and dissipate energy over time, making the C derivative well-suited for modeling viscoelastic materials or systems under long-term loading. The AB derivative introduces a broader, more persistent memory effect

governed by the Mittag-Leffler function, resulting in an extended influence of past deformations. As depicted in Figure 3, the radial displacement u changes more gradually and is sustained over a longer period, especially in systems with complex boundary conditions. This makes the AB derivative ideal for modeling materials with heterogeneous properties or structures under variable loading conditions. The CT derivative modifies the traditional memory effect by incorporating a tempering parameter, which exponentially reduces the influence of past deformations. This leads to a more localized and faster response, as seen in Figure 2, where the displacement field adjusts quickly to applied forces. The CT derivative is particularly suitable for applications requiring rapid mechanical response and minimal residual deformation, such as in dynamic systems or materials used in high-speed environments.

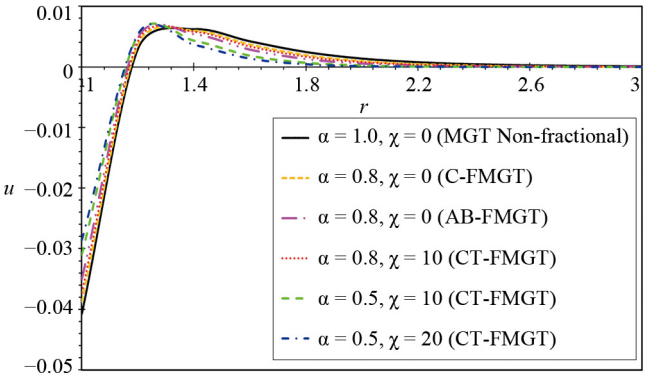

Figure 3. Displacement variation (u) under various fractional derivative operators

Figures 4 and 5 highlight how the type of fractional derivative used in the system significantly affects the behavior of thermal stress fields (σ_{rr} and $\sigma_{\psi\psi}$), particularly radial and hoop stresses. These stress fields are crucial in understanding material responses under thermal and mechanical loads. The Caputo derivative, with its power-law memory effect, causes a gradual buildup and slow release of thermal stresses, resulting in extended periods of stress relaxation. This makes it suitable for applications requiring controlled stress dissipation, though it may lead to sustained internal stresses. In contrast, the AB derivative introduces a more generalized and prolonged memory effect, leading to slower stress relaxation and increased stress accumulation, as observed in Figures 4 and 5. This extended influence of past stress states can increase the material's susceptibility to fatigue and failure, particularly under cyclic or long-term loading conditions.

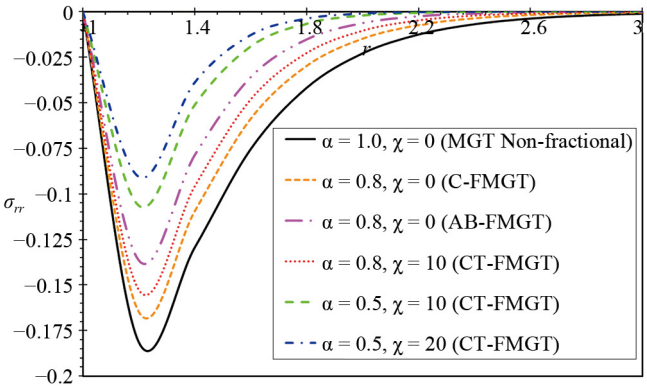

Figure 4. Radial stress variation (σ_{rr}) under various fractional derivative operators

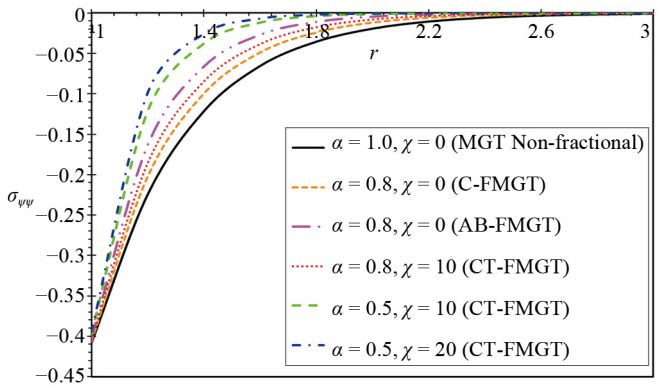

Figure 5. Hoop stress variation ($\sigma_{\psi\psi}$) under various fractional derivative operators

The CT derivative modifies the traditional memory effect by incorporating a tempering parameter that reduces the influence of past stresses. As Figures 4 and 5 show, this results in quicker stress relaxation and less long-term accumulation, making it ideal for high-performance materials and systems where rapid stress relief and durability are critical. Each derivative offers distinct benefits depending on the application, whether for slow, controlled stress dissipation, detailed long-term stress modeling, or rapid stress relaxation to prevent material degradation.

Figure 6 clearly demonstrates that carrier density N, reflecting the concentration of charge carriers like electrons or holes in a material, is influenced by thermal and electrical fields, which play a crucial role in the performance of electronic and photonic devices. The behavior of carrier density varies depending on the type of fractional derivative applied, C, AB, or CT. The Caputo derivative introduces a power-law memory effect, causing a delayed response in carrier density to external stimuli, as it is influenced by the entire history of past states. This results in a gradual evolution of carrier density, making it ideal for applications that benefit from sustained electrical or thermal activity, such as sensors or energy storage devices.

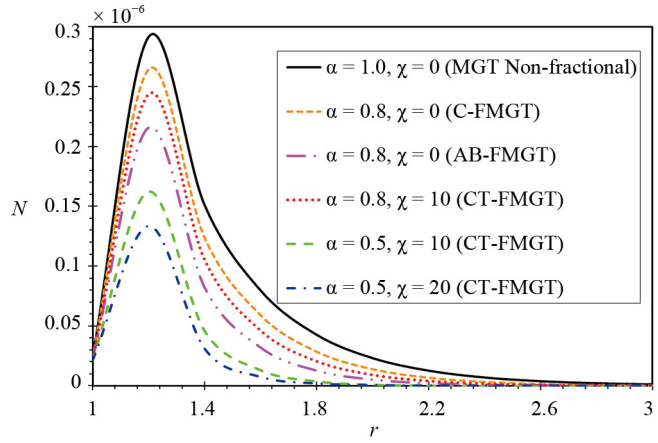

Figure 6. Carrier density variation (N) under various fractional derivative operators

The AB derivative, as shown in Figure 6, introduces a more prolonged memory effect, leading to an even slower response and greater charge density retention over time. This characteristic is particularly advantageous for applications like non-volatile memory devices, where maintaining high levels of charge density is essential. Lastly, as displayed in

Figure 6, the CT derivative, with its tempering parameter, reduces the long-term memory effect, enabling a faster response and quicker return to equilibrium. This rapid adjustment makes it well-suited for applications requiring fast response times, such as real-time sensors and high-speed electronics.

In the PTMGT model, the application of the Caputo derivative introduces a strong memory effect, leading to a slow response across all physical fields. This sluggish response is attributed to the system's prolonged retention of past thermal, mechanical, and electromagnetic states. Consequently, as illustrated in Figures 2 through 6, the temperature, displacement, stress, and carrier density fields evolve gradually, displaying a significant delay in reacting to changes within the system. The mechanical and electromagnetic fields also exhibit extended interactions, deeply influenced by historical events.

In contrast, when the AB fractional derivative is applied, it introduces a generalized memory effect, resulting in a more complex and non-local response in the physical fields. In this case, as shown in the various figures, the temperature, displacement, stress, and carrier density fields demonstrate a more intricate evolution, characterized by smoother transitions yet with a prolonged influence of past states. The results clearly indicate that the AB derivative broadens the temporal and spatial impact of these fields, leading to more complex interactions. This complexity is evident in how the fields respond, with a more nuanced and widespread influence of historical data on current states.

The Caputo tempered fractional derivative alters the traditional Caputo derivative by incorporating a tempering parameter, represented by χ. This parameter reduces the long-term memory effect typically associated with the Caputo derivative. Essentially, χ introduces an exponential decay factor that gradually lessens the impact of past states over time, leading to a quicker reduction in memory effects. This adjustment allows for more controlled and adaptable modeling in systems where limiting the persistence of historical effects is necessary, resulting in a faster return to equilibrium compared to the standard Caputo derivative. As a result, the Caputo tempered fractional derivative is especially valuable in applications that require a balance between memory retention and rapid stabilization.

When the CT fractional derivative is incorporated into the PTMGT photothermal model, it includes an exponential damping factor that accelerates the reduction of the influence of past states. This results in quicker stabilization of the temperature, displacement, stress, and carrier density fields, with a faster return to equilibrium compared to the other two derivatives. The analysis suggests that the CT fractional derivative is particularly effective in systems where a rapid response is desired, and where minimizing residual effects from past events is critical. This makes it an ideal choice for applications requiring quick stabilization and minimal lingering impacts from previous states.

The numerical results clearly show that memory effects in systems described by the Caputo tempered derivative are less pronounced over extended periods compared to those governed by the traditional Caputo derivative. The presence of the exponential factor $e^{-\chi t}$ reduces the impact of older states, resulting in a more localized memory effect over time. This tempered memory in the CT fractional operator is particularly advantageous for modeling physical processes where the influence of distant past events needs to diminish more quickly, such as in materials with time-dependent properties that stabilize over time.

9. Conclusion

This work presents a novel framework for photothermal conduction that combines the Moore-Gibson-Thomson equation with the Fourier law of thermal conduction, employing various fractional operators in place of traditional integer derivatives. The framework incorporates different fractional derivatives, such as Caputo (C), Atangana-Baleanu (AB), and tempered Caputo (CT), enabling the modeling of a broad spectrum of memory effects-from simple power-law decay to more complex non-local behaviors in semiconductor materials. The primary aim of this model is to deepen our understanding of the interactions between heat, plasma, and elastic waves in semiconductor materials while exploring non-local phenomena influenced by memory effects. By comparing this new approach with existing photothermal elasticity models, we can effectively evaluate its accuracy and performance in real-world applications involving semiconductor materials.

Some of the key conclusions that can be extracted from this paper include:

• Fractional derivatives play a crucial role in accurately capturing memory effects in materials with complex thermal behaviors, offering a more precise representation of heat conduction over time. By incorporating fractional derivatives into heat conduction models, time-dependent terms that account for the history of thermal processes are included, leading to more detailed and realistic simulations.

• Different types of fractional derivatives, such as Caputo (C), Atangana-Baleanu (AB), and Caputo tempered (CT), provide varying levels of memory effects, ranging from simple power-law decays to intricate non-local behaviors. This versatility allows for the modeling of a wide array of thermal processes.

• The choice of fractional derivative significantly influences the evolution of physical fields like temperature, displacement, stress, and carrier density, shaping how these fields respond to external stimuli over time:

•• The Caputo derivative introduces a power-law memory effect, resulting in slower, more gradual changes in physical fields, making it suitable for systems that require a sustained response.

•• The AB derivative produces a more complex and extended memory effect, leading to even slower, more prolonged changes in physical fields, ideal for applications where long-term stability and detailed non-local interactions are essential.

•• The CT derivative strikes a balance between memory and faster decay, leading to quicker stabilization of physical fields, making it suitable for systems that demand rapid response and minimal residual effects.

• Fractional derivatives are particularly valuable for simulating thermal processes in materials that exhibit anomalous diffusion and other non-classical behaviors, enhancing the understanding and development of advanced materials. Selecting the appropriate fractional derivative allows for precise control and prediction of thermal behavior in materials, tailored to specific application needs, whether requiring sustained activity or rapid adaptation.

• The integration of fractional derivatives into heat conduction models represents a significant advancement in simulation techniques, enabling more sophisticated and accurate predictions of material behavior under varying thermal conditions.

Author contributions

All authors discussed the results, reviewed and approved the final version of the manuscript.

Conflict of interest

The authors declare that they have no conflict of interest regarding the publication of the research article.

References

[1] Muratikov KL, Glazov AL, Rose DN, Dumar AJ. Photoacoustic effect in stressed elastic solids. *Journal of Applied Physics*. 2000; 88(5): 2948-2955.

[2] Cheng H, Zeng F, Zhang X, Tang J, Zhang Y. The effect of the photoacoustic field-photoacoustic cell coupling term on the performance of the gas detection system. *Optics and Laser Technology*. 2022; 153(6): 108211.

[3] Shrestha B, DeLuna F, Anastasio MA, Yong YJ, Brey EM. Photoacoustic imaging in tissue engineering and regenerative medicine. *Tissue Engineering Part B: Reviews*. 2020; 26(1): 79-102.

[4] Mallidi S, Luke GP, Emelianov S. Photoacoustic imaging in cancer detection, diagnosis, and treatment guidance. *Trends in Biotechnology*. 2011; 29(5): 213-221.

[5] Gu Y, Sun Y, Wang X, Li H, Qiu J, Lu W. Application of photoacoustic computed tomography in biomedical imaging: A literature review. *Bioengineering and Translational Medicine*. 2023; 8(2): e10419.

[6] Zafar M, Avanaki K. Laser scanning photoacoustic microscopy system for oxy/deoxy hemoglobin imaging. In *Photons Plus Ultrasound: Imaging and Sensing 2024, Vol. 12842*. USA: SPIE BiOS; 2024.

[7] Wu Y, Fu X, Li J, Zhang P, Wang H, Li Z. All-fiber photoacoustic system for large-area nondestructive testing. *Structural Health Monitoring*. 2024; 23(4): 2123-2134.

[8] Nowacki W. *Thermoelasticity*. Amsterdam, Netherlands: Elsevier; 2013.
[9] Pitarresi G, Patterson EA. A review of the general theory of thermoelastic stress analysis. *The Journal of Strain Analysis for Engineering Design*. 2003; 38(5): 405-417.
[10] Auriault JL. Cattaneo-vernotte equation versus fourier thermoelastic hyperbolic heat equation. *International Journal of Engineering Science*. 2016; 101: 45-49. Available from: http://dx.doi.org/10.1016/j.ijengsci.2015.12.002.
[11] Speziale CG. On the coupled heat equation of linear thermoelasticity. *Acta Mechanica*. 2001; 150(1): 121-126.
[12] Hetnarski RB, Ignaczak J. Nonclassical dynamical thermoelasticity. *International Journal of Solids and Structures*. 2000; 37(1-2): 215-224.
[13] Guo SL, Zhang YX, Wang KF, Wang BL, Zhang CW. Effects of non-fourier heat conduction and surface heating rate on thermoelastic waves in semi-infinite ceramics subject to thermal shock. *Ceramics International*. 2021; 47(12): 17494-17501.
[14] Lord HW, Shulman Y. A generalized dynamical theory of thermoelasticity. *Journal of the Mechanics and Physics of Solids*. 1967; 15(5): 299-309.
[15] Green AE, Naghdi P. On undamped heat waves in an elastic solid. *Journal of Thermal Stresses*. 1992; 15(2): 253-264.
[16] Green AE, Naghdi P. Thermoelasticity without energy dissipation. *Journal of Elasticity*. 1993; 31(3): 189-208.
[17] Choudhuri SKR. On a thermoelastic three-phase-lag model. *Journal of Thermal Stresses*. 2007; 30(3): 231-238.
[18] Tzou DY. The generalized lagging response in small-scale and high-rate heating. *International Journal of Heat and Mass Transfer*. 1995; 38(17): 3231-3240.
[19] Tzou DY. *Macro-to Microscale Heat Transfer: The Lagging Behavior*. USA: John Wiley and Sons; 2014.
[20] Elzayady ME, Abouelregal AE, Megahid SF. Analysis of porous magneto-thermoelastic solid cylinder via dual phase lag heat transfer model. *Pramana*. 2024; 98(1): 19.
[21] Abouelregal AE, Elmasry Y. Thermomagnetic modeling of a nonlocal viscoelastic half-space exposed to an internal heat source through a two-phase delay model. *Waves in Random and Complex Media*. 2024; 3(3): 1923-1944.
[22] Sun H, Zhang Y, Baleanu D, Chen W, Chen Y. A new collection of real world applications of fractional calculus in science and engineering. *Communications in Nonlinear Science and Numerical Simulation*. 2018; 64: 213-231. Available from: https://doi.org/10.1016/j.cnsns.2018.04.019.
[23] Dalir M, Bashour M. Applications of fractional calculus. *Applied Mathematical Sciences*. 2010; 4(21): 1021-1032.
[24] Magin RL, Ingo C, Colon-Perez L, Triplett W, Mareci TH. Characterization of anomalous diffusion in porous biological tissues using fractional order derivatives and entropy. *Microporous and Mesoporous Materials*. 2013; 178: 39-43. Available from: https://doi.org/10.1016/j.micromeso.2013.02.054.
[25] Alsaeed SS, Abouelregal AE, Elzayady ME. Magneto-thermoelastic responses in an unbounded porous body with a spherical cavity subjected to laser pulse heating via an Atangana-Baleanu fractional operator. *Case Studies in Thermal Engineering*. 2024; 61(4): 104968.
[26] Bavi O, Hosseininia M, Heydari MH, Bavi N. SARS-CoV-2 rate of spread in and across tissue, groundwater and soil: A meshless algorithm for the fractional diffusion equation. *Engineering Analysis With Boundary Elements*. 2022; 138(4): 108-117.
[27] Salem MG, Abouelregal AE, Elzayady ME, Sedighi HM. Biomechanical response of skin tissue under ramp-type heating by incorporating a modified bioheat transfer model and the Atangana-Baleanu fractional operator. *Acta Mechanica*. 2024; 235(8): 5041-5060.
[28] Owolabi KM. Computational study for the caputo sub-diffusive and riesz super-diffusive processes with a fractional order reaction-diffusion equation. *Partial Differential Equations in Applied Mathematics*. 2023; 8: 100564. Available from: https://doi.org/10.1016/j.padiff.2023.100564.
[29] Mainardi F. *Fractional Calculus and Waves in Linear Viscoelasticity: An Introduction to Mathematical Models*. Singapore: World Scientific; 2022.
[30] Zhang Y, Liu X, Lei D, Yin M, Sun H, Guo Z, et al. Modeling hydrologically mediated hot moments of transient anomalous diffusion in aquifers using an impulsive fractional-derivative equation. *Water Resources Research*. 2024; 60(3): e2023WR036089.
[31] Ross B. *Fractional Calculus and Its Applications: Proceedings of the International Conference Held at the University of New Haven, Vol. 457*. Heidelberg: Springer; 2006.
[32] Yang Y, Zhang HH. *Fractional Calculus With Its Applications in Engineering and Technology*. Berlin, Germany: Springer Nature; 2022.

[33] Baleanu D, Diethelm K, Scalas E, Trujillo JJ. *Fractional Calculus: Models and Numerical Methods, Vol. 3*. Singapore: World Scientific; 2012.
[34] Caputo M, Fabrizio M. A new definition of fractional derivative without singular kernel. *Progress in Fractional Differentiation and Applications*. 2015; 1(1): 73-85.
[35] Caputo M, Fabrizio M. Applications of new time and spatial fractional derivatives with exponential kernels. *Progress in Fractional Differentiation and Applications*. 2016; 2(1): 1-11.
[36] Atangana A, Baleanu D. Caputo-Fabrizio derivative applied to groundwater flow within confined aquifer. *Journal of Engineering Mechanics*. 2017; 143(5): D4016005.
[37] Atangana A, Baleanu D. New fractional derivatives with nonlocal and non-singular kernel: Theory and application to heat transfer model. *Thermal Science*. 2016; 20(2): 763-769.
[38] Amir FIA, Moussaoui A, Shafqat R, El Omari MH, Melliani S. The Hadamard Ψ-Caputo tempered fractional derivative in various types of fuzzy fractional differential equations. *Soft Computing*. 2024; 28: 1-18. Available from: https://doi.org/10.1007/s00500-024-09821-w.
[39] Zhao L, Li C, Zhao F. Efficient difference schemes for the Caputo-tempered fractional diffusion equations based on polynomial interpolation. *Communications on Applied Mathematics and Computation*. 2021; 3(1): 1-40.
[40] Guan W, Cao X. A numerical algorithm for the Caputo tempered fractional advection-diffusion equation. *Communications on Applied Mathematics and Computation*. 2021; 3(17): 41-59.
[41] Zhang J, Tang Y. A fast Euler-Maruyama scheme and its strong convergence for multi-term Caputo tempered fractional stochastic differential equations. *Communications in Nonlinear Science and Numerical Simulation*. 2024; 138: 108253. Available from: https://doi.org/10.1016/j.cnsns.2024.108253.
[42] Yadav AK. Photothermal plasma wave in the theory of two-temperature with multi-phase-lag thermo-elasticity in the presence of magnetic field in a semiconductor with diffusion. *Waves in Random and Complex Media*. 2022; 32(5): 2416-2444.
[43] Song YQ, Bai JT, Ren ZY. Study on the reflection of photothermal waves in a semiconducting medium under generalized thermoelastic theory. *Acta Mechanica*. 2012; 223(7): 1545-1557.
[44] Song Y, Todorovic DM, Cretin B, Vairac P. Study on the generalized thermoelastic vibration of the optically excited semiconducting microcantilevers. *International Journal of Solids and Structures*. 2010; 47(14-15): 1871-1875.
[45] Choi JH, Yoon SH, Park SG, Choi SH. Analytical solution of the Cattaneo-Vernotte equation (non-Fourier heat conduction). *Journal of Advanced Marine Engineering and Technology*. 2016; 40(5): 389-396.
[46] Abouelregal AE, Zakaria K, Sirwah MA, Ahmad H, Rashid AF. Viscoelastic initially stressed microbeam heated by an intense pulse laser via photo-thermoelasticity with two-phase lag. *International Journal of Modern Physics C*. 2022; 33(06): 2250073.
[47] Abouelregal AE. Modified fractional photo-thermoelastic model for a rotating semiconductor half-space subjected to a magnetic field. *Silicon*. 2020; 12(12): 2837-2850.
[48] Abouelregal AE, Sedighi HM, Sofiyev AH. Modeling photoexcited carrier interactions in a solid sphere of a semiconductor material based on the photothermal Moore-Gibson-Thompson model. *Applied Physics A*. 2021; 127(11): 845.
[49] Conti M, Pata V, Pellicer Sabadí M, De Latorre RQ. A new approach to MGT-thermoviscoelasticity. *Discrete and Continuous Dynamical Systems. Series A*. 2021; 41(10): 4645-4666.
[50] Tiwari R, Sachan S, Abouelregal A, Kumar R, Elzayady ME. Viscothermoelastic vibrations on circular microplate resonators using the Moore-Gibson-Thompson thermal-conductivity model. *Mechanics of Time-Dependent Materials*. 2024; 28(3): 1291-1311.
[51] Abouelregal AE, Sedighi HM, Megahid SF. Photothermal-induced interactions in a semiconductor solid with a cylindrical gap due to laser pulse duration using a fractional MGT heat conduction model. *Archive of Applied Mechanics*. 2023; 93(6): 2287-2305.
[52] Abouelregal AE, Rayan A, Mostafa DM. Transient responses to an infinite solid with a spherical cavity according to the MGT thermo-diffusion model with fractional derivatives without nonsingular kernels. *Waves in Random and Complex Media*. 2022; 1-29. Available from: https://doi.org/10.1080/17455030.2022.2147242.
[53] Oliveira DS, de Oliveira EC. On a Caputo-type fractional derivative. *Advances in Pure and Applied Mathematics*. 2019; 10(2): 81-91.
[54] Almeida R, Martins N, Sousa JVDC. Fractional tempered differential equations depending on arbitrary kernels. *AIMS Mathematics*. 2024; 9(4): 9107-9127.

[55] Obeidat NA, Rawashdeh MS. Theories of tempered fractional calculus applied to tempered fractional Langevin and Vasicek equations. *Mathematical Methods in the Applied Sciences*. 2023; 46(8): 8582-8595.
[56] Abouelregal AE, Ahmad H, Elagan SK, Alshehri NA. Modified Moore-Gibson-Thompson photo-thermoelastic model for a rotating semiconductor half-space subjected to a magnetic field. *International Journal of Modern Physics C*. 2021; 32(12): 2150163.
[57] Abouelregal AE, Atta D. A rigid cylinder of a thermoelastic magnetic semiconductor material based on the generalized Moore-Gibson-Thompson heat equation model. *Applied Physics A*. 2022; 128(2): 1-14.
[58] Elzayady ME, Abouelregal AE, Alsharif F, Althagafi H, Alsubhi M, Alhassan Y. Two-stage heat-transfer modeling of cylinder-cavity porous magnetoelastic bodies. *Mechanics of Time-Dependent Materials*. 2024; 28(4): 2819-2840.
[59] Liu L. An energy formulation of continuum magneto-electro-elasticity with applications. *Journal of the Mechanics and Physics of Solids*. 2014; 63(1): 451-480.
[60] Abouelregal AE, Marin M. The size-dependent thermoelastic vibrations of nanobeams subjected to harmonic excitation and rectified sine wave heating. *Mathematics*. 2020; 8(7): 1128.
[61] Abouelregal AE, Marin M, Alharbi HA, Alrouili KJ. Modeling the thermal behavior of functionally graded media with a spherical gap: Rectified sine wave heating via fourth-order Moore-Gibson-Thompson model. *Mechanics of Time-Dependent Materials*. 2024; 28(3): 681-707.
[62] Yablonovitch E, Allara DL, Chang CC, Gmitter T, Bright TB. Unusually low surface-recombination velocity on silicon and germanium surfaces. *Physical Review Letters*. 1986; 57(2): 249.
[63] Durbin F. Numerical inversion of Laplace transforms: An efficient improvement to Dubner and Abate's method. *The Computer Journal*. 1974; 17(4): 371-376.
[64] Valsa J, Brančik L. Approximate formulae for numerical inversion of Laplace transforms. *International Journal of Numerical Modelling: Electronic Networks, Devices and Fields*. 1998; 11(3): 153-166.
[65] Abouelregal AE, Alsaeed SS, Sedighi HM, Elzayady ME, Hafezi AR. A comprehensive study on heterogeneous media with spherical cavity: The higher-order fractional triple-phase-lag thermoelasticity with local kernels. *International Journal of Applied Mechanics*. 2024; 2450120. Available from: https://doi.org/10.1142/S1758825124501205.
[66] Marin M, Abbas I, Kumar R. Relaxed saint-venant principle for thermoelastic micropolar diffusion. *Structural Engineering and Mechanics*. 2014; 51(4): 651-662.
[67] Vlase S, Marin M, Scutaru ML, Száva IR. Coupled transverse and torsional vibrations in a mechanical system with two identical beams. *AIP Advances*. 2017; 7(6): 065301.
[68] Marin M, Öchsner A, Bhatti MM. Some results in Moore-Gibson-Thompson thermoelasticity of dipolar bodies. *ZAMM-Journal of Applied Mathematics and Mechanics*. 2020; 100(12): e202000090.
[69] Honig G, Hirdes U. A method for the numerical inversion of Laplace transforms. *Journal of Computational and Applied Mathematics*. 1984; 10(1): 113-132.